The relationship between clustering and networked Turing patterns

Cite as: Chaos 34, 073114 (2024); doi: 10.1063/5.0195450
Submitted: 2 January 2024 · Accepted: 19 June 2024 ·
Published Online: 8 July 2024

Xiaofeng Luo,[1,a)] Guiquan Sun,[1,2,3,a)] Runzi He,[1] Zhen Jin,[2,3] Joshua Kiddy K. Asamoah,[4,5] Yakui Xue,[1] and Lili Chang[2,3,a)]

AFFILIATIONS

[1]School of Mathematics, North University of China, Shanxi, Taiyuan 030051, China
[2]Complex Systems Research Center, Shanxi University, Shanxi, Taiyuan 030006, China
[3]Key Laboratory of Complex Systems and Data Science of Ministry of Education, Taiyuan 030006, China
[4]Department of Mathematics, Saveetha School of Engineering SIMATS, Chennai 602105, India
[5]Department of Mathematics, Kwame Nkrumah University of Science and Technology, Kumasi 127901, Ghana

[a)]**Authors to whom correspondence should be addressed:** luoxiaofeng@nuc.edu.cn; sunguiquan@nuc.edu.cn; and changll@amss.ac.cn

ABSTRACT

Networked Turing patterns often manifest as groups of nodes distributed on either side of the homogeneous equilibrium, exhibiting high and low density. These pattern formations are significantly influenced by network topological characteristics, such as the average degree. However, the impact of clustering on them remains inadequately understood. Here, we investigate the relationship between clustering and networked Turing patterns using classical prey–predator models. Our findings reveal that when nodes of high and low density are completely distributed on both sides of the homogeneous equilibrium, there is a linear decay in Turing patterns as global clustering coefficients increase, given a fixed node size and average degree; otherwise, this linear decay may not always hold due to the presence of high-density nodes considered as low-density nodes. This discovery provides a qualitative assessment of how clustering coefficients impact the formation of Turing patterns and may contribute to understanding why using refuges in ecosystems could enhance the stability of prey–predator systems. The results link network topological structures with the stability of prey–predator systems, offering new insights into predicting and controlling pattern formations in real-world systems from a network perspective.

Studies have shown that network topology significantly affects the Turing pattern formation in a networked reaction–diffusion (RD) system. Clustering is a common occurrence in nature, such as animals gathering for food and humans coming together to travel, work and celebrate festivals. Yet, the assessment of its impact on pattern formation remains little known. This research qualitatively analyzes the impact of the clustering coefficient, a crucial topological property of networks, on networked pattern formation.

I. INTRODUCTION

Patterns exist widely in the nature, such as spatiotemporal patterns (like target waves[1–3] and rotating spiral waves[1,4]) and stationary patterns (like Turing patterns[5–9]). The activator–inhibitor systems governed by reaction–diffusion (RD) equations have been well used to describe the pattern formation,[5–15] since Turing proposed and proved the Turing instability.[16] Turing indicated that the difference in diffusion coefficients between the activator and the inhibitor brings about the destabilization of the homogeneous state and leads to spontaneous periodic spatial patterns. It provides a classical mechanism of self-organization far from equilibrium, having been extensively applied in biological,[6,17] chemical,[5,8] and ecological systems.[7,18]

Up to now, the activator–inhibitor systems based on RD have been investigated mainly in continuous media[5–9,17,18] and discrete media.[10–15,19–22] Considering some real scenarios in biological and epidemiological systems, the latter is, to some extent, more applicable. For example, human or animal habitat patches (such as cities or lakes) distribute discretely in space, and individuals move or diffuse through the connections between the discrete habitats. In general,

the real systems considered in discrete media are often represented by the complex networks,[10–15,20] where nodes represent the habitats, assigned the density of activators and inhibitors in network RD systems, and edges represent the connections between habitats. In the early days, a general mathematical framework depicting Turing instability in networks has been proposed by Othmer and Scriven[22] but limited to the regular lattices or small networks. More recently, work in this field has been extensively extended in large networks with complex topological structures.[10–12,15,20]

Research has indicated that network topological structure significantly impacts the Turing pattern formation in complex networks.[10,12,20] For instance, in 2010, Nakao and Mikhailov studied the theory of Turing pattern formation in the random undirected networks, which displays the grouped structure patterns based on the node degree.[12] Asllani *et al.*[23] then extended the theory to the case of directed networks. They found that the directed network topology resulted in a new instability class at variance with the case in undirected networks. Asllani *et al.*[10] and Kouvaris *et al.*[20] discovered that the coupled structures in multiplex networks lead to heterogeneous patterns with significant differences from those observed in single-layer networks. Asllani *et al.*[24] showed that patterns of a network-organized RD system could be created or destroyed by tuning the network topology. Mimar *et al.*[25] extensively analyzed the relationship between network topology and the dynamical parameters and presented new insights into the nature of Turing patterns in network-organized RD systems. In a word, currently in most of the research studies, Turing patterns of networks are shown in the form of the stationary state of activators or inhibitors based on the size order of node degrees. Essentially, they reflect the effects of degree distribution on the Turing pattern formations in networks. Remarkably, Change *et al.* have found the exponential decay of pattern formation with the average degree.[26] Bram *et al.* found that a decrease in the average shortest distance increases the spectral gap of the Laplacian spectrum and consequently decreases the chances for Turing instability.[27,28] The average degree or the average shortest distance is only two of topological properties of networks. The clustering coefficients[29]—another property having equal importance with degree distribution in networks, have rarely been paid attention to studying Turing pattern formations.

The clustering coefficients could depict the degree of probability of my friend's friend being also my friend. In topological terms, it characterizes the proportion of loops of length three in the networks. Research has indicated that most of the systems in the real world have a high degree of clustering.[30] Thus, it is pretty important and necessary to study how the clustering affects the formation of Turing patterns in networks, and this is the aim of our present work.

This paper qualitatively analyzed the influences of clustering on Turing patterns based on classical RD systems.[18,31,32] Our results showed that nodes in the low-density group of network patterns and the amplitude of network patterns decrease linearly with an increase in the clustering coefficients when nodes of high and low density for activator are completely distributed on both sides of the homogeneous state for given a fixed node size and average degree. Otherwise, this linear decay may break due to the presence of high-density nodes below the homogeneous state. This might provide the researcher with evidence that establishing the refuge of preys is conducive to stabilize the prey–predator systems.[33–35] It gives us a new insight into preventing and controlling Turing pattern formations in the biological, ecological, and epidemiological systems.

The rest of this paper is organized as follows. In Sec. II, we gave the global and local clustering coefficients and the clustered networks. In Secs. III and IV, we introduced the classical RD systems and performed the bifurcation analysis. In Sec. V, we plotted Turing patterns based on clustering coefficients, and analyzed and formalized the linear-like decay relations between the clustering coefficients and Turing patterns. Finally, we ended with discussion and conclusion.

II. THE CLUSTERING COEFFICIENTS AND GENERATED NETWORKS

This section introduces the general forms of global and local clustering coefficients, and then provide the generated clustered networks and the possible range of clustering coefficients within these networks for a fixed average degree and node size.

An adjacent matrix $A = (a_{ij})_{N\times N}$ could generally describe a simple and undirected network with N individuals. Here, $a_{ij} = 1$ if node i and node j are connected ($i \neq j$); $a_{ij} = 0$, otherwise. The global clustering coefficient of this network ϕ could be expressed by the adjacent matrix A,[36] i.e.,

$$\phi = \frac{Number\ of\ loops\ of\ length\ three}{Number\ of\ paths\ of\ length\ two} = \frac{trace(A^3)}{||A^2|| - trace(A^2)}. \quad (1)$$

It represents the ratio between the number of loops of length three and the number of paths of length two in the network (see Fig. 1). If the degree of a single node i in the network and the number of actual connected edges between node i's neighbors are separately denoted by k_i and e_i, the local clustering coefficient ϕ_i for the node i could be defined as

$$\phi_i = \frac{Number\ of\ loops\ of\ length\ three\ through\ node\ i}{Number\ of\ paths\ of\ length\ two\ through\ node\ i} = \frac{2e_i}{k_i(k_i-1)}, \quad (2)$$

where $k_i = \sum_{j=1}^{N} a_{ij}$.[37,38] It represents the ratio between the number of loops of length three through node i and the number of paths of length two through node i (see Fig. 1).

In the paper, we take two classic networks of node size 1000 with a high degree of clustering and tunable clustering coefficients as the base networks (see the illustration with 27 nodes in Fig. 2).

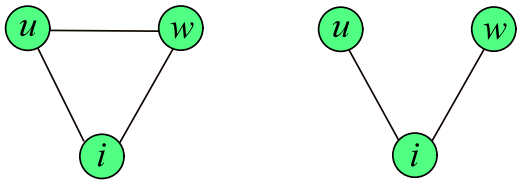

FIG. 1. Illustration of a loop of length three and a path of length two. The path *uiw* is said to be a loop of length three if the third edge directly from *u* to *w* is present (solid edges), otherwise be a path of length two.

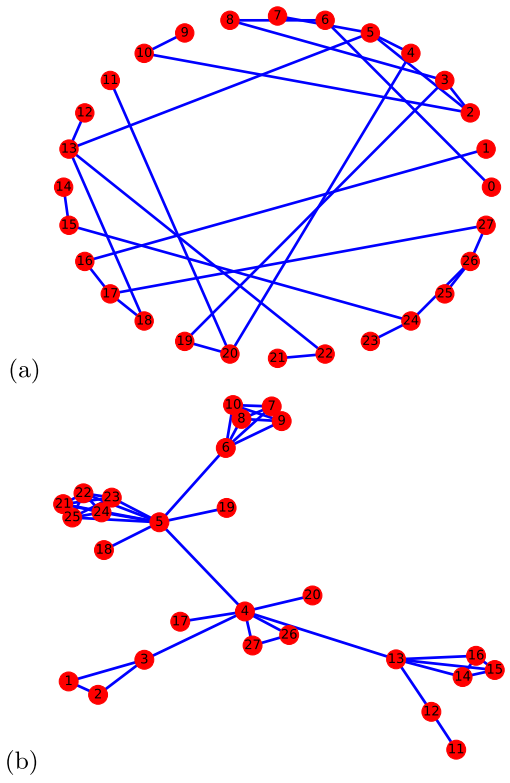

FIG. 2. Illustration of two clustered networks : (a) WS small-world network and (b) GP clustered network.

One is the small-world network of Watts and Strogatz (WS),[30] and the other is the randomly configuration clustered network proposed by J. P. Gleeson (GP) in Ref. 39 We first briefly introduce the GP clustered network. It comprises a series of cliques (a fully connected subgraph), and especially, a single node is regarded as 1-clique. Each node in the network is at most a member of one clique and has two types of edges: internal edges belonging to one clique and external edges not belonging any clique. In other words, this type of network could be decomposed into disjoint cliques regarded as the supernode. It then could be generated by connecting randomly chosen pairs of the external link stubs of nodes in all supernodes based on the configured random networks.[40] For example, the GP clustered network in Fig. 2(b) contains four individual nodes 17, 18, 19, and 20 (could be regarded as 1-clique); one 2-clique with nodes 11 and 12; two 3-clique with nodes 1, 2, and 3 and nodes 4, 26, and 27; one 4-clique with nodes 13, 14, 15, and 16; one 5-clique with nodes 6, 7, 8, 9, and 10; and one 6-clique with nodes 5, 21, 22, 23, 24, and 25. These cliques or supernodes are then are connected to form the GP clustered network in Fig. 2(b) by randomly choosing and connecting external edges (4,3), (4,5), (4,13), (4,17), (4,20), (5,6), (5,18), (5,19), and (12,13).

As for the generated process of the two types of networks, we use the function *sample_smallworld* of the igraph package in R to generate the WS small-world network with different global clustering coefficients by changing the rewiring probability p. Specifically, we adopt the dimension of the starting lattice and the size of the lattice as 1 and 1000, respectively. For the GP clustered network, to ensure a larger clustering coefficient, we choose the combination of the individual node (1-clique) and 30-clique to generate the GP clustered network with different global clustering coefficients by tuning the number of 30-clique (NC) (because the remaining nodes are the 1-clique).

It is important to note that clustering coefficients have a limited range given node size and average degree of a network. We then explore the broadest spectrum of clustering coefficients in the WS small-world network with parameter p ranging from 0 to 1, and the GP clustered network characterized by a variation in NC from 1 to 33, which signifies the upper limit of 30-cliques (see Table I). It could be observed in Table I that, in the WS small-world network, the clustering coefficient range expands as the average degree increases from 10 to 30. Beyond this point, the range begins to contract, with the maximum coefficient values stabilizing around 0.74 for degrees between 30 and 700, whereas the minimum values escalate rapidly due to the increasing average degree. After 700, the range becomes less than 0.1 although there is a higher value. We, thus, choose the case of an average degree of 30 for the WS small-world network, which has the widest range of clustering coefficients from 0.032 to 0.735. In the GP clustered network, as the NC increases, the range generally widens before reaching an average degree of 30. After this point, the range decreases to less than 0.1. This is because, beyond an average degree of 30, most edges, except those belonging to the 30-clique, participate in random configurations, resulting in a smaller clustering coefficient.[40] Thus, we focus on the case of an average degree of 30 in the GP clustered network, which has the widest range of clustering coefficients from 0.056 to 0.921. Figure 3 shows the specific range of clustering coefficients for average degree

TABLE I. The range of clustering coefficients generated for various average degrees in the WS small-world network with $p \in [0, 1]$ and in the GP clustered network with NC $\in$[1, 33].

Average degree	Range of clustering coefficients	
	WS small-world network ($p \in [0, 1]$)	GP clustered network (NC$\in$[1, 33])
10	[0.010, 0.645]	[0.021, 0.650]
20	[0.021, 0.701]	[0.036, 0.850]
30	[0.032, 0.735]	[0.056, 0.921]
40	[0.043, 0.736]	[0.063, 0.243]
70	[0.070, 0.738]	[0.074, 0.209]
110	[0.111, 0.740]	[0.113, 0.159]
150	[0.152, 0.743]	[0.151, 0.173]
200	[0.245, 0.746]	[0.201, 0.211]
300	[0.324, 0.747]	[0.300, 0.304]
500	[0.515, 0.749]	[0.502, 0.503]
700	[0.751, 0.774]	[0.701, 0.701]
800	[0.851, 0.861]	[0.890, 0.893]
900	[0.921, 0.937]	[0.933, 0.942]

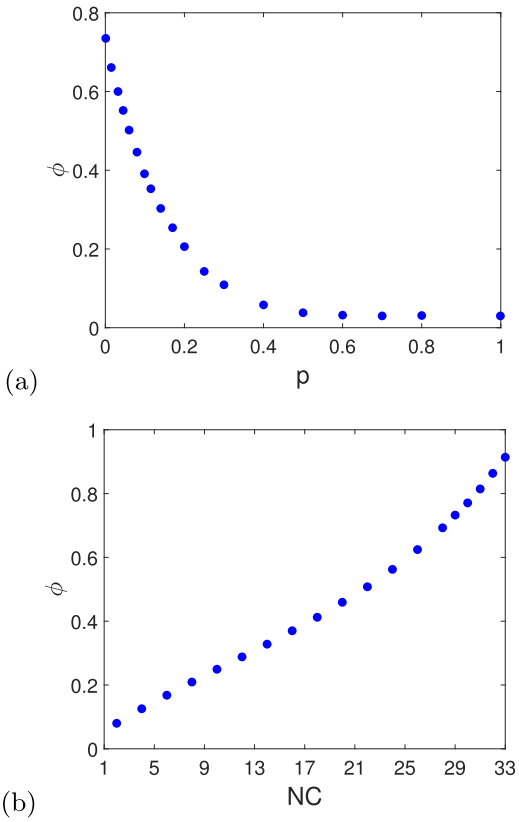

FIG. 3. The clustering coefficients in the case of average degree 30 with the change in (a) the rewiring probability p in the WS small-world network and (b) the number of 30-clique (NC) in the GP clustered network.

30 and node size 1000 in the WS small network [refer to Fig. 3(a)] and GP clustered network [see Fig. 3(b)].

Furthermore, whether for a fixed rewiring probability in a WS small-world network or for a combination of different types of cliques in a GP clustered network, the clustering coefficients of generated networks fluctuate slightly. We, thus, generate 30 networks for one given rewiring probability or clique combination to calculate the average global clustering coefficients. We investigate the average dynamical behavior of the Turning pattern formation in these networks.

III. DYNAMICAL MODEL

In this section, we first review the general form of a network-organized RD system in discrete media and then introduces the two classical prey–predator systems.

A network-organized RD system often takes the following form:

$$\begin{aligned} \frac{du_i}{dt} &= f(u_i, v_i) + \varepsilon \sum_{j=1}^{N} l_{ij} u_j, \\ \frac{dv_i}{dt} &= g(u_i, v_i) + \sigma\varepsilon \sum_{j=1}^{N} l_{ij} v_j, \end{aligned} \tag{3}$$

where $u_i(t), v_i(t), i = 1, \ldots, N$ represent the activator and inhibitor concentration in node i, f and g stand for the generic nonlinear reaction terms, and ε and $\sigma\varepsilon$ label the diffusion coefficients of the activator and inhibitor, respectively. Different from continuous media, the Laplacian operator is replaced by the Laplacian matrix $L = (l_{ij})_{N\times N}$ of a network in discrete media, where

$$l_{ij} = a_{ij} - \delta_{ij} k_i, \tag{4}$$

and δ_{ij} is a Kronecker delta function,[12,23] satisfying $\delta_{ij} = 1$ if and only if $i = j$; otherwise, $\delta_{ij} = 0$.

To precisely evaluate the influence of the clustering coefficients on pattern formation, we choose two classical models in the following to validate the universality of our results.

(1) Gierer–Meinhardt (GM) model:[31] $f(u, v) = u^2/v - u, g(u, v) = Gu^2 - Ev$ with the equilibrium point, $(u^*, v^*) = (E/G, E/G)$. It depicted the molecular mechanism of the pattern formation of tissue in morphogenesis based on auto- and cross catalysis between activators and inhibitors.

(2) Mimura–Murray (MM) model:[12,18] $f(u, v) = [(a + bu - u^2)/c - v]u$, $g(u, v) = [u - (1 + dv)]v$. It explained the phenomenon that the diffusion distinction between preys and predators results in the spatial patchiness in plant–herbivore systems.

IV. BIFURCATION ANALYSIS

In what follows, we perform the detailed calculation by the linear analysis to obtain the Turing bifurcation.

Let (u^*, v^*) be a locally stable positive equilibrium point of system (3) defined by $f(u^*, v^*) = 0$, $g(u^*, v^*) = 0$. We introduce small perturbations to the equilibrium (u^*, v^*) at node i as

$$u_i = u^* + \delta u_i, \quad v_i = v^* + \delta v_i. \tag{5}$$

Substituting (5) in Eq. (3) and linearizing, one obtains the linearized system as follows:

$$\begin{cases} \dfrac{\mathrm{d}\delta u_i}{\mathrm{d}t} = f_u \delta u_i + f_v \delta v_i + \varepsilon \displaystyle\sum_{j=1}^{N} l_{ij} \delta u_j, \\ \dfrac{\mathrm{d}\delta v_i}{\mathrm{d}t} = g_u \delta u_i + g_v \delta v_i + \sigma\varepsilon \displaystyle\sum_{j=1}^{N} l_{ij} \delta v_j, \end{cases} \tag{6}$$

where f_u, f_v, g_u, and g_v denote the partial derivatives at the equilibrium.

Let μ_s be the eigenvalue corresponding an eigenvector of the Laplacian matrix, $\Phi^{(s)} = (\phi_1^{(s)}, \phi_2^{(s)}, \ldots, \phi_N^{(s)})^T$, $s = 1, \ldots, N$. Note that the Laplacian matrix of a undirected network L is a real, symmetric, and negative semi-definite matrix, so its eigenvalues are real,

non-positive. Expanding the perturbations in the basis formed by eigenvectors of the Laplacian matrix, i.e.,

$$(\delta u_i,\ \delta v_i) = \sum_{s=1}^{N} \left(c_s^1,\ c_s^2\right) e^{\lambda_s t} \phi_i^{(s)}, \tag{7}$$

then substituting (7) into (6) and using $L\Phi^{(s)} = \mu_s \Phi^{(s)}$, we obtain, for each mode s,

$$\lambda_s \begin{pmatrix} c_s^1 \\ c_s^2 \end{pmatrix} = \begin{pmatrix} f_u + \varepsilon\mu_s & f_v \\ g_u & g_v + \sigma\varepsilon\mu_s \end{pmatrix} \begin{pmatrix} c_s^1 \\ c_s^2 \end{pmatrix}. \tag{8}$$

The corresponding characteristic equation of system (6) becomes

$$\lambda_s^2 - p(\mu_s)\lambda_s + q(\mu_s) = 0, \tag{9}$$

where

$$p(\mu_s) = f_u + g_v + \varepsilon(1+\sigma)\mu_s,$$
$$q(\mu_s) = f_u g_v - f_v g_u + \varepsilon(g_v + \sigma f_u)\mu_s + \sigma\varepsilon^2\mu_s^2.$$

Therefore, the linear growth rates λ_s, the eigenvalues of system (6), are

$$\lambda_{s,1} = \frac{p(\mu_s) + \sqrt{p(\mu_s)^2 - 4q(\mu_s)}}{2},$$
$$\lambda_{s,2} = \frac{p(\mu_s) - \sqrt{p(\mu_s)^2 - 4q(\mu_s)}}{2}. \tag{10}$$

For Turing bifurcation, it is indispensable to satisfy the condition that the equilibrium point is stable for the model without diffusion, while it becomes unstable when diffusion is considered.[41] It follows that the critical condition of the Turing bifurcation satisfies

$$\mathrm{Im}(\lambda_s) = 0, \quad \mathrm{Re}(\lambda_s) = 0, \ \text{at}\ \ \mu_s = \mu_s^T \neq 0.$$

That is, $q(\mu_s^T) = 0$ with

$$\mu_s^T = -\sqrt{\frac{q(0)}{\sigma\varepsilon^2}}.$$

Then, it is easily obtained that

$$\left.\frac{d\lambda_{s,2}}{d\mu_s}\right|_{\mu_s=\mu_s^T} = \frac{\varepsilon(1+\sigma)}{2} - \frac{\varepsilon(1+\sigma)}{2} = 0,$$
$$\left.\frac{d^2\lambda_{s,2}}{d\mu_s^2}\right|_{\mu_s=\mu_s^T} = \frac{\left[2q(0) + \varepsilon(g_v + \sigma f_u)\right]^2}{f_u + g_v + \varepsilon(1+\sigma)\mu_s^T} < 0.$$

It means that system (6) has one eigenvalue $\lambda_{s,2}$, of which the real-part will increase to be positive from the negative number symmetrically via the judgment on convexity and concave (referring to Fig. 4). Therefore, the system experiences the destabilization induced by diffusion, i.e., the Turing bifurcation occurs and the corresponding pattern emerges.

According to the analysis of Turing bifurcation above, the parameters of the GM model are set to, $\varepsilon = 0.01$, $\sigma = 1/\varepsilon$, $G = 3$, $E \in \{9,\ 10.5,\ 12\}$, and the parameters of the MM model are set to, $a = 35$, $b = 16$, $c = 9$, $d = 0.4$, $\varepsilon = 0.03$, and $\sigma \in \{30,\ 35,\ 40\}$ with an equilibrium point $(u^*, v^*) = (5, 10)$.

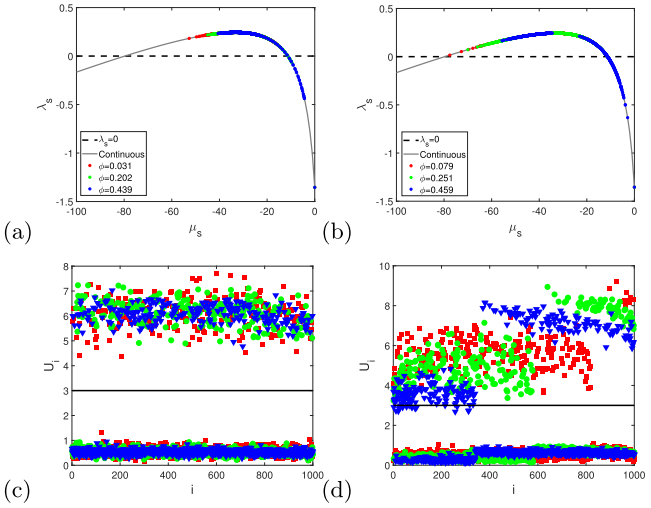

FIG. 4. For the GM model ($E = 9$) in the generated networks in Sec. II, (a) and (b) show the dispersion relation for the WS and GP networks with three different global clustering coefficients, and the gray curve represents the continuous case; (c) and (d) show the stationary patterns of activators as a function of node index i for three global clustering coefficients corresponding to (a) and (b) in WS small-world and GP clustered networks, where nodes are sorted according to their ascending local clustering coefficients. (a) and (c) correspond to WS small-world network, and (b) and (d) correspond to the GP clustered network. The black line represents the homogeneous state $u^* = 3$ of the GM model ($E = 3$).

Taking the case of $E = 9$ in the GM model as an example, Figs. 4(a) and 4(b) show the evolution of the linear growth rate λ_s as a function of Laplacian eigenvalues μ_s in the generated WS small-world and GP clustered networks with different clustering coefficients in Sec. II. It shows a linear growth rate satisfying $\lambda_s > 0$.

V. MAIN RESULTS

A. Turing patterns in networks

In this section, based on the above parameter settings of Turing instability conditions of GM and MM models, we carry out numerical simulation in the generated WS small-world network and GP clustered network in Sec. II for the case of average degree 30 and node size 1000. To explore the network patterns in different global clustering coefficients, the initial conditions of those two models are set to small perturbations around the positive equilibrium point, that is,

$$u_i(0) = u^* + 0.0005 \times \eta_i, \quad v_i(0) = v^* + 0.0005 \times \eta_i, \tag{11}$$

where η_i, $i = 1, \ldots, N$, follows the standard normal distribution $N(0, 1)$. It is given in advance and keeps constant in the whole process.

To be displayed clearly in Figs. 4(c) and 4(d), the stationary Turing patterns of the activator as a function of node index i for the GM model ($E = 9$) only consider three global clustering coefficients (0.031, 0.079—red squares; 0.202, 0.251—green circles; 0.439, 0.459—blue triangles) corresponding to coefficients in Figs. 4(a)

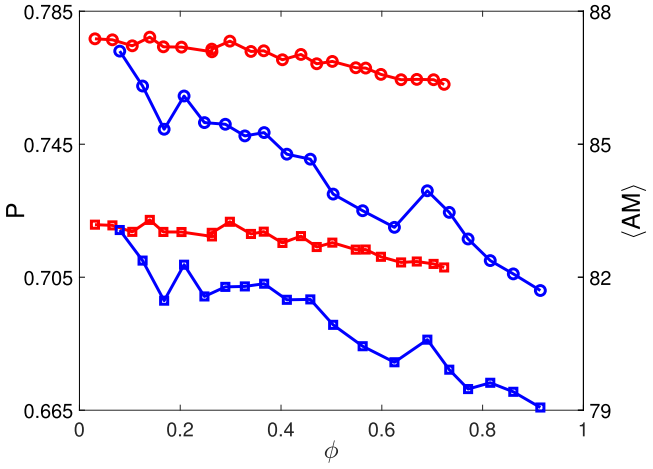

FIG. 5. The proportion of nodes in bottom group P (circle and left vertical scale) and the amplitude AM (square and right vertical scale) vs the global clustering coefficient ϕ for the GM model ($E = 9$) in the WS small-world network (red) and GP clustered network (blue).

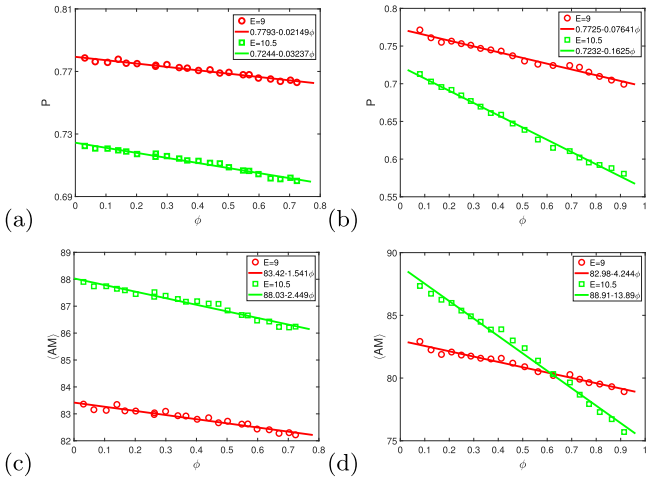

FIG. 6. The proportion of nodes in bottom group P and the amplitude AM as a function of global clustering coefficient ϕ for the GM model, and corresponding nonlinear regression $\hat{P} = a + b\phi$, $\hat{AM} = a_1 + b_1\phi$. (a) and (c) in the WS small-world network; (b) and (d) in the GP clustered network.

and 4(b), in particular, where nodes are sorted according to their ascending local clustering coefficients. It could be seen that (1) for each clustering coefficient, the activator presents an obvious grouped distribution formed by two groups of nodes: the top group with high density and the bottom group with low density. The number of nodes in the bottom group is greater than that in the top group; (2) the amplitude of nodes distributing at both sides of the uniform state line, especially in the top group, is larger in the case of $\phi = 0.031, 0.079$ than that in the case of $\phi = 0.202, 0.251$ in two networks. The least amplitude is in the case of $\phi = 0.439, 0.459$. Here, as many researches have done,[12,20,21] the stationary Turing patterns of inhibitor are not presented, because it is similar to the patterns of the activator.

Since the patterns of the nodes' grouped distribution in Figs. 4(c) and 4(d) are generated from the small perturbations around the homogeneous state $u^* = 3$, we denote the number and proportion of nodes below u^* as N_{bot} and P, respectively, to qualitatively describe the relationship between low-density nodes and clustering coefficients. We have

$$P = \frac{N_{bot}}{N}. \tag{12}$$

According to Refs. 12, 20, and 42, we also define the amplitude of non-uniform state of the activator as

$$AM = \left[\sum_{i=1}^{N} (u_i - u^*)^2\right]^{1/2}. \tag{13}$$

Figure 5 presents one of the 30 simulating results for these two quantities of the GM model ($E = 9$) in two types of networks in Sec. II. Interestingly, we find that the proportion of nodes in bottom group and amplitude of the activator has a nearly linear decrease with an increase in the global clustering coefficients.

TABLE II. Parameters of linear regression for the GM model in two types of networks given a fixed average degree of 30 and a node size of 1000.

Network	E	$a \in$ CI (95%)	$b \in$ CI (95%)	R^2
WS	9	$0.7793 \in [0.7785, 0.7802]$	$-0.02149 \in [-0.02335, -0.01962]$	0.9665
	10.5	$0.7244 \in [0.7233, 0.7255]$	$-0.03237 \in [-0.03481, -0.02993]$	0.9746
GP	9	$0.7725 \in [0.7694, 0.7755]$	$-0.07641 \in [-0.08204, -0.07079]$	0.9797
	10.5	$0.7232 \in [0.7197, 0.7266]$	$-0.1625 \in [-0.1688, -0.1562]$	0.9943
Network	E	$a_1 \in$ CI (95%)	$b_1 \in$ CI (95%)	R^2
WS	9	$83.42 \in [83.34, 83.50]$	$-1.541 \in [-1.722, -1.361]$	0.9409
	10.5	$88.03 \in [87.94, 88.12]$	$-2.449 \in [-2.659, -2.238]$	0.9671
GP	9	$82.98 \in [82.80, 83.17]$	$-4.244 \in [-4.585, -3.902]$	0.9759
	10.5	$88.91 \in [88.54, 89.28]$	$-13.89 \in [-14.57, -13.21]$	0.9908

B. Linear decay induced by clustering coefficients

In what follows, we reveal the relationship between the number of nodes in the bottom group, the amplitude of the activator, and the global clustering coefficients.

As Sec. II described, to avoid the oscillated impacts of the clustering coefficients for a fixed rewiring probability in the WS small-world network and a combination of cliques in GP clustered network on the simulated results, we generate 30 networks for one given rewiring probability or a combination of cliques to calculate the averages of global clustering coefficients, the corresponding proportion of nodes in the bottom group and the amplitude. One arbitrary experiment is plotted in Figs. 5 for the GM model. It is clearly shown that the proportion P and amplitude AM almost decrease linearly in the increase in the global cluster coefficient ϕ. Naturally, it could be a good choice to apply the linear regression model,

$$\hat{P} = a + b\phi, \tag{14}$$

$$\hat{AM} = a_1 + b_1\phi, \tag{15}$$

to fit discrete points (ϕ, P) and (ϕ, AM). The fitting results by using the least square method are the solid lines plotted in Fig. 6.

It is intuitively seen that nonlinear regression models (14) and (15) match the discrete points very well, which is also validated by the fitting parameters shown in Table II. The fitted values of a, b, a_1, b_1 and corresponding 95% confidence intervals are listed in the third and fourth columns. The fitting goodness $R^2 > 0.90$ in the fifth column indicates a high fitting degree of the nonlinear regression models. These regression results clearly demonstrate that the proportion of nodes in the bottom group and the amplitude for the GM model present a law of linear-like decay when increasing global clustering coefficients given the fixed average degree and node size. Likewise, Fig. 7 presents the similar results for the MM model and the fitting parameters are shown in Table III. The outstanding fitting goodness, indicated by an R^2 value greater than 0.90 in the fifth column, also signifies a high degree of fitting for the MM model.

However, as indicated in Ref. 26, when the average degree is small, nodes with high and low density do not always completely distribute on either side of the homogeneous state u^* for some models. For example, in a sample case with an average degree of 12 in a WS small-world network, Figs. 8(a) and 8(b) present the patterns for the GM model (left side) and MM model (right side). Here, the parameters of the two models are the same as before, and the clustering coefficients range from 0 to 0.68 according to Table I. It can be seen that some high-density nodes in the top group are located below the homogeneous state u^* (indicated by the black solid line). Interestingly, in this case, we find that the linear decay always holds in the GM model [see Fig. 8(c)] but breaks in the MM model [see Fig. 8(d)]. This phenomenon is also reflected in the amplitudes of the two models, though not presented here to avoid repetition. Why does this happen? Observing patterns in the case of an average degree of 12 shown in Figs. 8(a)–8(b) and in the case of an average degree of 30 shown in Fig. 4(c) in the WS small-world network, the sole difference is that some high-density nodes below u^* have been regarded as low-density nodes in the case of an average degree of 12. We hypothesize that these nodes may cause the linear decay to break in

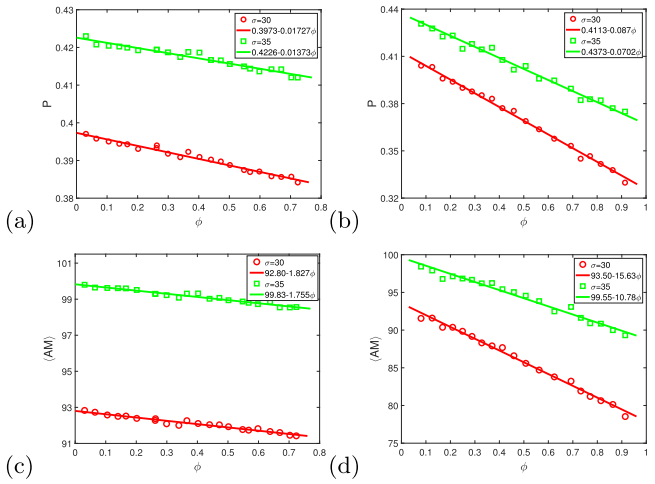

FIG. 7. The proportion of nodes in bottom group P and the amplitude AM as a function of global clustering coefficient ϕ for the MM model, and corresponding nonlinear regression $\hat{P} = a + b\phi$, $\hat{AM} = a_1 + b_1\phi$. (a) and (c) The WS small-world network; (b) and (d) the GP clustered network.

TABLE III. Parameters of linear regression for the MM model in two types of networks given a fixed average degree of 30 and a node size of 1000.

Network	σ	$a \in$ CI (95%)	$b \in$ CI (95%)	R^2
WS	30	$0.3973 \in [0.3968, 0.3979]$	$-0.01727 \in [-0.01857, -0.01597]$	0.9747
	35	$0.4226 \in [0.4219, 0.4233]$	$-0.01373 \in [-0.01525, -0.01222]$	0.9470
GP	30	$0.4113 \in [0.4080, 0.4145]$	$-0.08702 \in [-0.09293, -0.0811]$	0.9827
	35	$0.4373 \in [0.4341, 0.4406]$	$-0.07022 \in [-0.07616, -0.06428]$	0.9734
Network	σ	$a_1 \in$ CI (95%)	$b_1 \in$ CI (95%)	R^2
WS	30	$92.80 \in [92.73, 92.88]$	$-1.827 \in [-1.998, -1.656]$	0.9614
	35	$99.83 \in [99.75, 99.91]$	$-1.755 \in [-1.937, -1.573]$	0.9528
GP	30	$93.50 \in [92.97, 94.02]$	$-15.63 \in [-16.59, -14.67]$	0.9857
	35	$99.55 \in [99.05, 100.10]$	$-10.78 \in [-11.70, -9.858]$	0.9729

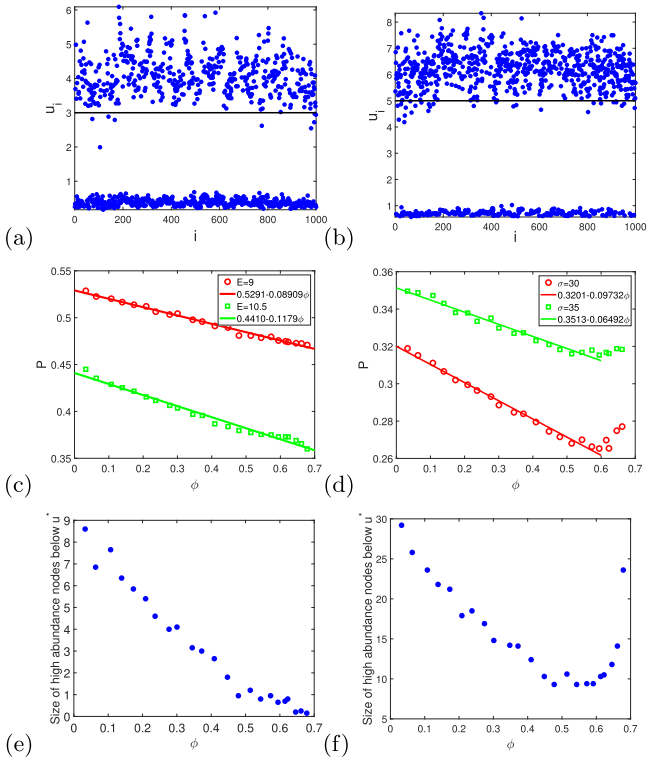

FIG. 8. Considering the case of average degree 12 in the WS small-world network for the GM model (left side) and MM model (right side). (a) and(b) present one sample of stationary patterns with $\phi = 0.052$ in two models; (c) and(d) represent the proportion of nodes in bottom group P as a function of global clustering coefficient ϕ and the nonlinear regression $\hat{P} = a + b\phi, \hat{AM} = a_1 + b_1\phi$; (e) and (f) show the size of high-density nodes between the homogeneous state u^*.

the MM model. To explore this hypothesis, we present the relationships between the average number of these high-density nodes below u^* and the clustering coefficients in Figs. 8(e) and 8(f) for the two models. We see that the trends in the number of these nodes with clustering coefficients in the two models are consistent with the fitness results [linear decay holding in the GM model and breaking in the MM model in Figs. 8(c) and 8(d)]. Similar simulations are conducted for other different average degrees according to Table I. They all demonstrate that when nodes of high and low density are completely distributed on both sides of the homogeneous state u^* , the proportion of nodes in the bottom group P and the amplitude AM in Turing patterns linearly decrease with the increase in the global clustering coefficient ϕ, given a fixed node size and average degree (see Figs. 6 and 7). Otherwise, this linear decay may break due to the presence of high-density nodes below the homogeneous state, as seen in the MM model in Fig. 8(d).

Combining all these observations, we conclude that the decay relationship of the Turing pattern with the clustering coefficient is a commonly shared characteristic in networked activator–inhibitor systems. In most cases, the result of the linear decrease in low-density nodes or the linear increase in high-density nodes with the increase of clustering supports the fact that, in ecosystems, the presence of refuges for prey strengthens their persistence and further ensures the sustainability of the corresponding prey–predator systems.[33–35] This finding underscores the importance of considering clustering effects in the design and analysis of ecological networks, as it provides valuable insights into the stability and resilience of these systems.

VI. DISCUSSION AND CONCLUSION

The clustering phenomenon, a collective behavior, widely exists in nature.[30] Unfortunately, it is not yet well understood how clustering affects the formation of Turing patterns in real-world systems. In this work, based on two classical RD systems in Refs. 17 and 31, we presented the node-grouped structure of Turing patterns according to the ascending order of local clustering coefficients [see Figs. 4(c) and 4(d)] in the generated WS small-world and randomly GP clustered networks in Sec. II. It depicts the impacts of the clustering on patterns, different from patterns according to the descending order of node degrees in Refs. 12, 19, and 25, which focused on the effects of degree distribution on patterns. We then defined the number of nodes in the bottom group denoted by N_{bot} in (12) and the activator amplitude represented by AM in (13). Furthermore, the linear regression models (14) and (15) are chosen by the quantitative analysis of node distribution in the top and bottom of groups to fit the discrete nodes. The fitting results are shown in Figs. 6–8 and Tables II and III. It demonstrates that when the grouped nodes with high and low density completely distribute on either side of the homogeneous state with the increase in average degrees, the proportion of nodes in the bottom group and the amplitude for GM and MM models have a law of linear decay with the increase in the global clustering coefficients for the given average degree and node size (see Figs. 6 and 7). Otherwise, this linear decay mechanism may break due to the presence of high-density nodes considered as low-density nodes (see Fig. 8). This finding provides new insights and guidelines for preventing and controlling pattern formation in biological, ecological, and epidemiological systems.

Studies have demonstrated that the prerequisites for Turing instability in prey–predator ecosystems can be met, indicating that Turing patterns may serve as a characteristic form of ecological self-organization.[7,12] As stated in Sec. I, ecosystems are represented in networks where nodes symbolize animals' fragmented habitats (e.g., cities or lakes), and individuals travel or diffuse along the connections between these habitats. The linear decay results in Figs. 6–8 show that the low-density group of activators representing the preys in the bottom declines as the global clustering coefficients grow. In other words, the high-density group of preys grows as their clustering intensifies, implying that when prey–predator ecosystems are highly clustered, prey populations become more stable. In reality, the result also applies to predators because the stationary Turing patterns of inhibitors are similar to those of activators in our research. The finding explains why the use of refuge for preys or predators contributes to the enhancement of prey–predator coexistence[33–35] because it essentially enhances the density of preys or predators to prevent their extinctions and keeps their overall clustering degree

at a high level. As an example, in the ecosystem,[34] the whelk *Thais* eats all the barnacles that settle low on the shores each year, but it is difficult to eat the barnacles on the higher shore due to the short period between low tides. As a result, the shore above this height forms a sanctuary for barnacles. The special habitat environment guarantees that barnacles have a relatively high degree of clustering, which contributes to the stability of this small prey–predator system.

In addition, the average shortest path is another network topological parameter. The variable also varies in accordance with the clustering coefficient when the network model parameter changes. To figure out its impact on the linear behavior, Fig. 9 illustrates the relationships between the clustering coefficient and the average shortest path by varying the network model parameters (rewiring probability in the WS small world network and the number of 30-clique (NC) in GP clustered network) according to Fig. 3. Each point corresponds to the clustering coefficient and the average shortest path of networks created using the same model parameter. We could notice that in WS small-world network, the average shortest path grows linearly with the clustering coefficient from 0 to roughly 0.4. Then, the growth rate between them increases rapidly, showing a nonlinear relationship. In a GP clustered network, the growth rate between the average shortest path and the clustering coefficient increases slowly. It indicates a nonlinear relationship between them but may also be seen as a linear relationship between 0 and approximately 0.4. Furthermore, according to the linear relation between the proportion of nodes in the bottom group, amplitude, and clustering coefficients in the GM and MM model (see Figs. 6 and 7), it could be naturally implied that there exists same nonlinear relationship between the proportion of nodes in the bottom group, amplitude, and the average shortest path as in Fig. 9. It allows us to dismiss the idea that the linear-like behavior is completely due to the average shortest path as it is difficult to determine the effects of the clustering coefficient and the average shortest path because of their linear-like relationship when the clustering coefficient takes 0 to roughly 0.4.

In conclusion, we provide a qualitative analysis on the impacts of clustering coefficients on networked Turing pattern formations based on the classical prey–predator RD systems in the clustering networks. It not only is conducive to understand some spontaneous formation of patterns due to population clustering in real-world systems but provides theoretical evidence for protecting the stability of prey–predator systems by increasing the clustering degree of the prey or predator, such as establishing refuges for the prey or predator. Nevertheless, our bifurcation analysis was limited to linear stability analysis and did not derive the explicit expression between the clustering coefficients and the pattern modes. The development of multiple-scale theory in clustering networks may help solve this problem, finding out the essential reasons for generating the linear-like decay mechanism of Turing patterns.

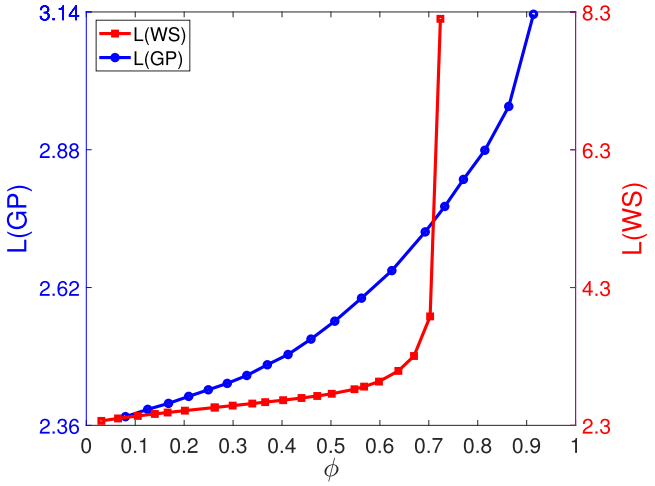

FIG. 9. The average shortest path (L) vs the global clustering coefficients at the same variation in the model parameters for WS small-world (red right side) and GP clustered (left blue side) networks based on Fig. 3.

ACKNOWLEDGMENTS

This research was supported by the National Natural Science Foundation of China (NNSFC) under Grant Nos. 12101573, 12022113, and 12231012, the Fundamental Research Program of Shanxi Province under Grant Nos. 20210302124381 and 20210302124608, the 19th Graduate Science and Technology Project of NUC under Grant No. 20231941, and the Key Research and Development Project of Lvliang under Grant No. 2022GXYF18.

AUTHOR DECLARATIONS

Conflict of Interest

The authors have no conflicts to disclose.

Author Contributions

Xiaofeng Luo: Conceptualization (equal); Funding acquisition (equal); Methodology (equal); Writing – original draft (equal). **Guiquan Sun:** Conceptualization (equal); Methodology (equal); Writing – review & editing (equal). **Runzi He:** Conceptualization (equal). **Zhen Jin:** Conceptualization (equal). **Joshua Kiddy K. Asamoah:** Conceptualization (equal). **Yakui Xue:** Conceptualization (equal). **Lili Chang:** Conceptualization (equal); Methodology (equal).

DATA AVAILABILITY

The data that support the findings of this study are available from the corresponding authors upon reasonable request.

REFERENCES

[1] S. Gui-Quan, J. Zhen, L. Quan-Xing, and L. Li, "Chaos induced by breakup of waves in a spatial epidemic model with nonlinear incidence rate," J. Stat. Mech.: Theory Exp. **2008**(08), P08011 (2008).
[2] R. G. Marcus and F. B. James, "A reaction-diffusion system of type part ii: Numerical analysis," Eur. J. Appl. Math. **16**(5), 621–646 (2005).
[3] R. G. Marcus, "Finite-difference schemes for reaction–diffusion equations modeling predator–prey interactions in MATLAB," Bull. Math. Biol. **69**(3), 931–956 (2007).
[4] R. G. Marcus and C. Trenchea, "Spatiotemporal dynamics of two generic predator-prey models," J. Biol. Dyn. **4**(6), 559–570 (2010).

[5]V. Castets, E. Dulos, J. Boissonade, and P. De Kepper, "Experimental evidence of a sustained standing Turing-type nonequilibrium chemical pattern," Phys. Rev. Lett. **64**(24), 2953 (1990).
[6]M. P. Harris, S. Williamson, J. F. Fallon, H. Meinhardt, and R. O. Prum, "Molecular evidence for an activator–inhibitor mechanism in development of embryonic feather branching," Proc. Natl. Acad. Sci. U.S.A. **102**(33), 11734–11739 (2005).
[7]J. L. Maron and S. Harrison, "Spatial pattern formation in an insect host-parasitoid system," Science **278**(5343), 1619–1621 (1997).
[8]Q. Ouyang and H. L. Swinney, "Transition from a uniform state to hexagonal and striped Turing patterns," Nature **352**(6336), 610–612 (1991).
[9]G.-Q. Sun, "Pattern formation of an epidemic model with diffusion," Nonlinear Dyn. **69**(3), 1097–1104 (2012).
[10]M. Asllani, D. M. Busiello, T. Carletti, D. Fanelli, and G. Planchon, "Turing patterns in multiplex networks," Phys. Rev. E **90**(4), 042814 (2014a).
[11]L. Chang, C. Liu, G. Sun, Z. Wang, and Z. Jin, "Delay-induced patterns in a predator–prey model on complex networks with diffusion," New J. Phys. **21**(7), 073035 (2019).
[12]H. Nakao and A. S. Mikhailov, "Turing patterns in network-organized activator-inhibitor systems," Nat. Phys. **6**(7), 544–550 (2010).
[13]J. Petit, M. Asllani, D. Fanelli, B. Lauwens, and T. Carletti, "Pattern formation in a two-component reaction-diffusion system with delayed processes on a network," Physica A **462**, 230–249 (2016).
[14]J. Petit, T. Carletti, M. Asllani, and D. Fanelli, "Delay-induced turing-like waves for one-species reaction-diffusion model on a network," Europhys. Lett. **111**(5), 58002 (2015).
[15]C. Tian and S. Ruan, "Pattern formation and synchronism in an allelopathic plankton model with delay in a network," SIAM J. Appl. Dyn. Syst. **18**(1), 531–557 (2019).
[16]A. M. Turing, "The chemical basis of morphogenesis," Philos. Trans. R. Soc. London **237**, 37–72 (1952).
[17]H. Meinhardt and A. Gierer, "Pattern formation by local self-activation and lateral inhibition," BioEssays **22**(8), 753–760 (2000).
[18]M. Mimura and J. D. Murray, "On a diffusive prey-predator model which exhibits patchiness," J. Theor. Biol. **75**(3), 249–262 (1978).
[19]L. Chang, M. Duan, G. Sun, and Z. Jin, "Cross-diffusion-induced patterns in an sir epidemic model on complex networks," Chaos **30**(1), 013147 (2020).
[20]N. E. Kouvaris, S. Hata, and A. Díaz-Guilera, "Pattern formation in multiplex networks," Sci. Rep. **5**(1), 1–9 (2015).
[21]C. Liu, L. Chang, Y. Huang, and Z. Wang, "Turing patterns in a predator-prey model on complex networks," Nonlinear Dyn. **99**, 1–10 (2020).
[22]H. G. Othmer and L. E. Scriven, "Instability and dynamic pattern in cellular networks," J. Theor. Biol. **32**(3), 507–537 (1971).
[23]M. Asllani, J. D. Challenger, F. S. Pavone, L. Sacconi, and D. Fanelli, "The theory of pattern formation on directed networks," Nat. Commun. **5**(1), 1–9 (2014b).
[24]M. Asllani, T. Carletti, and D. Fanelli, "Tune the topology to create or destroy patterns," Eur. Phys. J. B **89**(12), 1–10 (2016).
[25]S. Mimar, M. M. Juane, J. Park, A. P. Munuzuri, and G. Ghoshal, "Turing patterns mediated by network topology in homogeneous active systems," Phys. Rev. E **99**(6), 062303 (2019).
[26]L. Chang, L. Guo, C. Liu, Z. Wang, and G. Sun, "The qualitative and quantitative relationships between pattern formation and average degree in networked reaction-diffusion systems," Chaos **32**(9), 093129 (2022).
[27]A. S. Bram, L. H. Cameron, P. G. James, and A. Malbor, "Role of modularity in self-organization dynamics in biological networks," Phys. Rev. E **102**(5), 052306 (2020).
[28]A. Malbor, A. S. Bram, A. Alex, and P.G. James, "Symmetry-breaking mechanism for the formation of cluster chimera patterns," Chaos **32**(1), 013107 (2022).
[29]M. E. J. Newman, "Properties of highly clustered networks," Phys. Rev. E **68**(2), 026121 (2003b).
[30]D. J. Watts and S. H. Strogatz, "Collective dynamics of 'small-world' networks," Nature **393**(6684), 440–442 (1998).
[31]A. Gierer and H. Meinhardt, "A theory of biological pattern formation," Kybernetik **12**(1), 30–39 (1972).
[32]I. Prigogine and R. Lefever, "Symmetry breaking instabilities in dissipative systems. II," J. Chem. Phys. **48**(4), 1695–1700 (1968).
[33]J. H. Connell, "A predator-prey system in the marine intertidal region. i. Balanus glandula and several predatory species of thais," Ecol. Monogr. **40**(1), 49–78 (1970).
[34]W. W. Murdoch and A. Oaten, "Predation and population stability," Adv. Ecol. Res. **9**, 1–131 (1975).
[35]S. Sarwardi, P. K. Mandal, and S. Ray, "Analysis of a competitive prey–predator system with a prey refuge," BioSystems **110**(3), 133–148 (2012).
[36]M. J. Keeling, "The effects of local spatial structure on epidemiological invasions," Proc. R. Soc. B **266**(1421), 859–867 (1999).
[37]M. E. Newman, "The structure and function of complex networks," SIAM Rev. **45**(2), 167–256 (2003).
[38]M. E. J. Newman, *Networks: An Introduction* (Oxford University Press, 2010).
[39]J. P. Gleeson, "Bond percolation on a class of clustered random networks," Phys. Rev. E **80**(3), 036107 (2009).
[40]M. E. Newman, H. S. Steven, and J. W. Duncan, "Random graphs with arbitrary degree distributions and their applications," Phys. Rev. E **64**(2), 026118 (2001).
[41]G.-Q. Sun, C.-H. Wang, L.-L. Chang, Y.-P. Wu, L. Li, and Z. Jin, "Effects of feedback regulation on vegetation patterns in semi-arid environments," Appl. Math. Modell. **61**, 200–215 (2018).
[42]S. Hata, H. Nakao, and A. S. Mikhailov, "Dispersal-induced destabilization of metapopulations and oscillatory Turing patterns in ecological networks," Sci. Rep. **4**(1), 1–9 (2014).